Structural and magnetic properties of metastable $Fe_{1-x}Si_x$ ($0.15<x<0.34$) alloys prepared by a rapid-quenching technique

2002 J. Phys.: Condens. Matter 14 1985

(http://iopscience.iop.org/0953-8984/14/8/326)

INSTITUTE OF PHYSICS PUBLISHING JOURNAL OF PHYSICS: CONDENSED MATTER

J. Phys.: Condens. Matter **14** (2002) 1985–2000 PII: S0953-8984(02)27349-X

Structural and magnetic properties of metastable $Fe_{1-x}Si_x$ ($0.15 < x < 0.34$) alloys prepared by a rapid-quenching technique

L K Varga[1], F Mazaleyrat[2], J Kovac[3] and J M Greneche[4]

[1] Research Institute for Solid State Physics and Optics, 1525 Budapest POB 49, Hungary
[2] LESiR, ESA CNRS 8029, Ecole Normale Supérieure de Cachan, 94235 Cachan Cedex, France
[3] Institute of Experimental Physics, SAS, Watsonova 47, Kosice, Slovakia
[4] Laboratoire de Physique de l'Etat Condensé, UMR CNRS 6087, Université du Maine, 72085 Le Mans Cedex, France

Received 27 July 2001, in final form 17 January 2002
Published 15 February 2002
Online at stacks.iop.org/JPhysCM/14/1985

Abstract

$Fe_{1-x}Si_x$ ($0.15 < x < 0.375$) alloys have been prepared by a rapid-quenching technique. X-ray diffraction patterns show that these alloys consist of submicron grains between 100 and 300 nm. The DO_3 cubic symmetry could be obtained for Si content up to 34 at.% Si. This feature is particularly interesting since alloys containing more than 26 at.% Si and cast with usual techniques consist of a mixture of Fe_3Si and Fe_5Si_3. The magnetization, Curie temperature and resistivity data for these fine-grained alloys are consistent with those for bulk alloys for Si content below 25 at.% Si. In contrast, the structural and physical data for single-phase alloys with 28–34 silicon content are reported for the first time. Within this composition range, the magnetization and Curie point values roughly correspond to those suggested by the extrapolation of existing data. However, the resistivity shows an unexpected marked increase above 25 at.% Si. The values of resistivity, magnetization and effective anisotropy of soft-magnetic nanocrystalline Fe_2Si are found to be 200 $\mu\Omega$ cm, 0.6 T and 15 kJ m^{-3} respectively, suggesting that this alloy has potential for high-frequency applications.

(Some figures in this article are in colour only in the electronic version)

1. Introduction

Among the soft-magnetic alloys, Fe–Si was one of the earliest to be discovered. Indeed, Hadfield first observed the effect on mechanical properties of silicon additions to iron in 1882 for a sample containing an unexpected 1.5 wt% silicon. He also reported the benefit of this addition for the magnetic properties of iron in 1900 [1] and the mass production of Fe–Si sheets for transformer cores started in Germany in 1903.

The first investigations of high-Si-content Fe–Si alloys were in 1918, carried out by Gumlich [2], but the first publication which reports the Curie temperature values obtained over a very large concentration range (extending up to 30 at.% Si) is that of Murakami [3]. These results were confirmed and extended to a larger number of compositions by Fallot [4], who also added the corresponding values of the saturation magnetization M_S. However, both Murakami and Fallot's alloys, produced by copper mould casting and containing more than 25 at.% Si, were mixtures of Fe_3Si and Fe_5Si_3 stoichiometric compounds.

During the 1990s, much time was devoted to the production of non-equilibrium Fe–Si nanostructured powdered alloys by high-energy ball milling up to 45 at.% Si [5, 6]. Micro-sized powder with nano-sized grains of about 10 nm has already been achieved. Contrary to the expectations of good soft-magnetic properties due to the nanostructure, coercive fields of more than 2 kA m^{-1} were found over the whole composition range. This is probably due to the high internal stresses and structural defects and to the wide distribution of the powder grain sizes that result from the mechanical alloying process. The resistivity has not yet been reported, to our knowledge, as a function of Si content for powders obtained by mechanical alloying.

In recent years, great efforts have also been made to improve the magnetic properties of the Fe–Si alloys by rapid quenching [7–9]. Rapidly quenched $Fe_{88}Si_{12}$ (6.5 wt% Si–Fe) ribbons have been especially thoroughly investigated due to the nearly zero magnetostriction at this composition. Currently, commercial-scale production of this composition is also achieved by rolling and chemical-vapour-deposition (CVD) processes [10]. Below ∼12 at.% Si, the rapidly solidified and annealed microcrystalline alloys prove to be superior to the conventional grain-oriented steels at high induction [11]. At high Si content, above 12 at.% Si, the material becomes brittle and exhibited no features of practical interest until now. We are aware of amorphization of these alloys being attempted by four different routes: (i) vapour deposition of thin films (of $Fe_{70}Si_{30}$ and $Fe_{65}Si_{35}$) [12]; (ii) rapid quenching of thin films [13]; (iii) mechanical grinding of bulk materials [14]; and (iv) spark erosion [15].

With the increasing demands of powder core technologies, however, the study of 'bulk' ribbon alloys with high silicon content has become unavoidable. Further motivation is provided by the need for better understanding of the properties of the nanograins in the Finemet, one of the best soft-magnetic nanocrystalline materials [16]. Indeed, these two-phase alloys, obtained after a subsequent annealing treatment of the as-quenched amorphous precursor, consist of nanocrystalline grains dispersed within an amorphous residual phase. Both their proportions and compositions are strongly dependent on the annealing conditions (time and temperature) and on the initial composition. The chemical composition of these $Fe_{100-x}Si_x$ nanograins varies in the range $15 < x < 22$ at.% Si as a function of annealing temperature and time [17–19], but for this composition region (corresponding to the low-concentration side of off-stoichiometric DO_3 structure), little is known about the anisotropy and magnetostriction. In addition, FeAlSi grains with metalloid contents ranging from 19 up to 27 at.% have been found recently in nanocrystalline Al-containing Finemet [20].

In the high-silicon-content region there are two stoichiometric phases: α_1-Fe_3Si (DO_3) and η-F_5Si_3 (hexagonal, D_8) [21]. Below about 11 at.% Si, a solid solution of silicon in iron can be generally observed in its ordered (B2) and disordered (A2) forms. Between about 11 and 15 at.% Si a phase mixture of a solid solution of Si in bcc Fe (B2) and of the ordered DO_3 structure of the Fe_3Si compound was reported [22].

These developments posed two main questions: (i) what is the composition of the single-phase structure when the silicon content is higher than 25 at.%; and (ii) is it possible to achieve high resistivity in such alloys, retaining the interesting soft-magnetic properties? We suggest that the metastable state obtained by means of a rapid-quenching procedure should favour such features.

Recently, the possibility of producing single-phase metastable compounds by rapid quenching from the melt with Si atomic content up to 34% has been demonstrated [23]. Above this limit, the alloys consist of two phases. The present set of experiments show that the DO_3 structure persists from 15 to 34%, although traces of Fe_5Si_3 could also be detected [23]. The as-cast ribbons exhibit submicron grain size down to 100 nm for the highest silicon content. The metastable alloys (above $x = 0.25$) have resistivities as high as 180–220 $\mu\Omega$ cm, which is unusual for crystalline iron alloys. Special attention is paid to Fe_2Si, which shows very interesting properties at high frequencies. Due to its high resistivity (200 $\mu\Omega$ cm), the initial permeability of as-cast ribbons of this compound has a constant value of 250 up to 5 MHz, which is comparable to that for NiZn ferrite but with dramatic reduction in production cost. The coercive field is relatively high (150 A m^{-1}), but not really detrimental to HF application at low induction [23].

2. Experimental procedure

The starting alloy material was made from pure electrolytic iron (99.99%) and pure silicon (99.999%). Melting and casting were conducted by induction heating into a copper chill mould under argon. The ribbons were prepared from 20 g ingots by a planar-flow technique on a rotating steel wheel at 30 m s^{-1}. The as-cast ribbons were about 20 μm thick and 1 mm wide.

X-ray measurements were performed using cobalt radiation. The Co Kα_2 line was digitally filtered and the lattice parameters where calculated from the angular position of the main diffraction peak. In a second step, the spectra were fitted according the structure using Maud software based on the RITA/RISTA method [24] taking into account instrumental parameters. The fits of the whole patterns yield the lattice parameter, average grain size and subsequently the relative fraction of the different phases. The saturation magnetization was measured in a vibrating-sample magnetometer at 4.2 K and at 6 T magnetizing field. The Curie points were determined from thermomagnetic curves, by means of a Faraday balance, up to 800 °C in vacuum using a small field of 2400 A m^{-1}. The resistivity was measured using the four-points method. The section was calculated from mass and length measurements while the density was estimated from the cell constants. ^{57}Fe Mössbauer experiments were performed in transmission geometry using a conventional spectrometer with a constant-acceleration signal and a ^{57}Co source diffused into a rhodium matrix. The samples were located under vacuum in either a bath cryostat or a cryofurnace to register spectra at temperatures between 77 and 600 K. Ribbons were maintained perpendicular to the unpolarized γ-beam to get Mössbauer spectra, but some texture-free spectra were also obtained using the magic angle configuration to check on the effect of the texture of ferromagnetic domains, if any. The analysis of the Mössbauer spectra was done using the Mosfit program [25] and the values of isomer shift were quoted relative to that of bcc Fe at 300 K.

3. Results and discussion

3.1. Structural properties

Some selected x-ray patterns recorded on rapidly quenched Fe–Si ribbons are illustrated in figure 1: they show the presence of well-defined Bragg peaks, consistent with a crystalline structure. It is also concluded that the DO_3 structure clearly persists up to $x = 28$ at.% Si, as attested by superstructure peaks (111) and (200) of the DO_3 phase around $2\theta = 32°$ and 37°. The spectra for samples with $x = 0.32$–0.34 both exhibit a peak near 37° which could correspond to the (100) peak of a simple cubic phase (B2). Owing to the very high

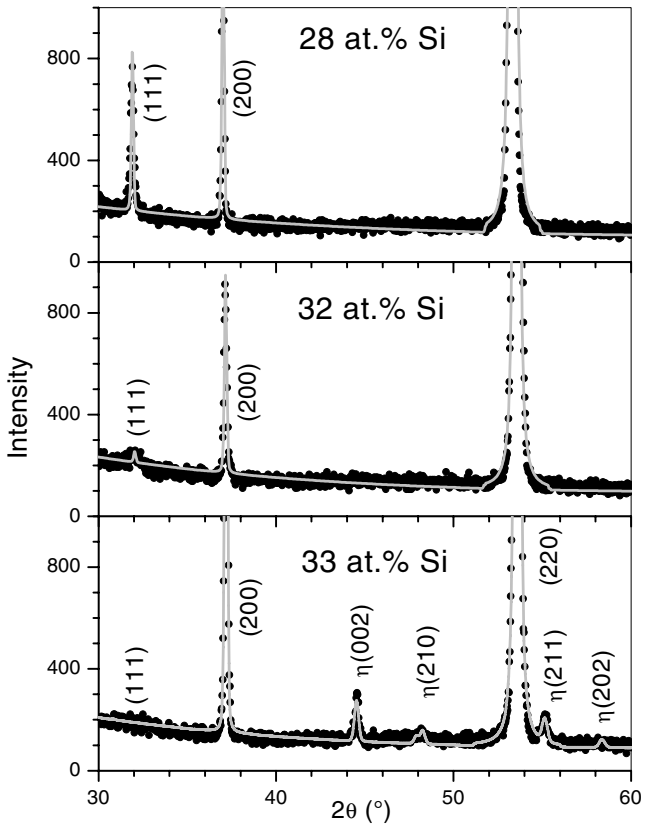

Figure 1. An enlarged view of some x-ray patterns of FeSi alloys with 28, 32 and 33 at.% Si. The points are experimental and the solid curve is the fit computed by Maud software.

quality of present spectra however, a very small peak around 32° is detected. This indicates that the structures of these samples are not totally disordered. Indeed, the DO_3 structure of stoichiometric Fe_3Si can be decomposed into two elementary cubic subnetworks: one containing Fe atoms only and a second composed of alternating Fe and Si atoms. If $x > 0.25$, the first subnetwork contains randomly substituted Si atoms. For instance, in Fe_2Si, one in six of the Fe atoms of the first subnetwork are replaced by Si, which induces subsequent deviation from stoichiometry, yielding a weak (111) superstructure peak. Another explanation could be a narrow distribution of composition. Indeed, a slight deviation from the nominal composition is induced by the precipitation of a small fraction of η-Fe_5Si_3 (0, 2 and 8% for $x = 0.32, 0.33, 0.34$ respectively). Figure 2 depicts the lattice parameters computed using Maud while refined values of the structural data are listed in table 1. The linear dependence on silicon content is in agreement with literature data [26], but the present values show a 0.6 pm constant offset. In order to clear up this discrepancy, we have calculated the lattice parameter by a classical technique, i.e. with the Bragg condition applied to the main line, here the (200) line. In this case, the calculated values corresponded with those found in the literature. Obviously, the modern methods are more accurate, because the structure is taken into account and an eventual offset is removed. However, the 2% shift in the present case can lead to small errors in the chemical analysis. The average grain size is between 95 and 280 ± 30 nm, but does not show a trend. It is interesting to note that one particular sample with 31 at.% Si displays two phases: DO_3 Fe–Si and 15% of hexagonal Fe_5Si_3, probably due to inadequate control of the

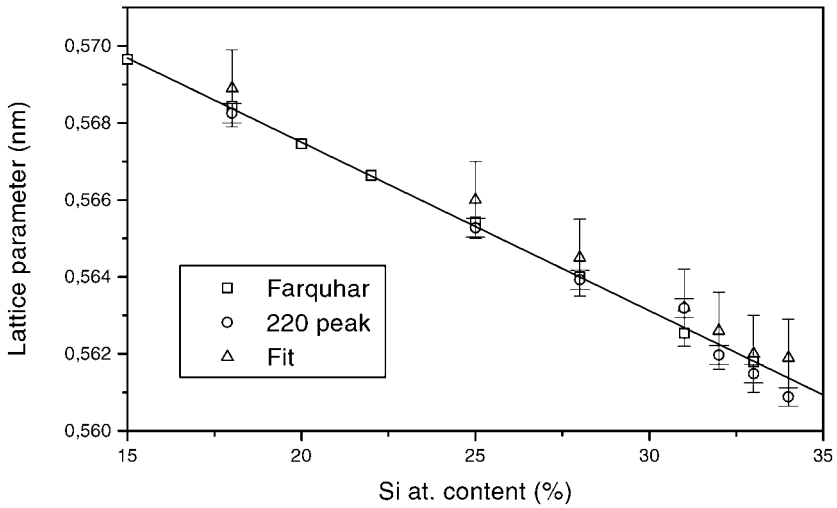

Figure 2. Lattice parameter as a function of silicon content. Present work: ○, calculated from the (200) line angular position; △, computed from a fit to the structure. Reference [26]: □, for convenience, the lattice parameters are multiplied by a factor of 2; the line is guide to the eyes.

Table 1. Structural characteristics as a function of silicon content.

Si (at.%)	a (nm), ± 0.0005	Grain size (nm), ± 30
18	0.5689	224
25	0.5660	170
28	0.5645	278
31	0.5632	95
32	0.5626	177
33	0.5620	200
34	0.5619	139

quenching conditions. The smaller grain size of this sample (100 nm) is probably due to the competition between the two phases, which impede each other in grain growth.

In the following sections, we report the composition dependence of the physical properties of $Fe_{1-x}Si_x$ alloys, which have been investigated for samples having a metastable structure with a well or slightly ordered DO_3 structure.

3.2. Electrical resistivity

Values of the electrical resistivity already reported in the literature [27, 28] are presented in figure 3. In the single-phase bcc solid solution (A2), the resistivity increases almost linearly with concentration up to about 12 at.% Si. In the mixed two-phase region (B2 + DO_3), between about 12 and 20 at.% Si, the steepness of the increase is reduced. The drop towards the Fe_3Si stoichiometric composition starting around 20 at.% is explained by DO_3 ordering. In the present samples however, the resistivity starts decreasing slightly from 15 at.%, which is due to the superstructure already present in the rapidly quenched ribbons. After 25 at.% a steep rise in resistivity is observed, with unusual values for a crystalline metal (150–220 $\mu\Omega$ cm). The thermal coefficient of resistivity (TCR) has been found to be positive over the whole compositional range, although the samples with $x > 0.31$ surpass

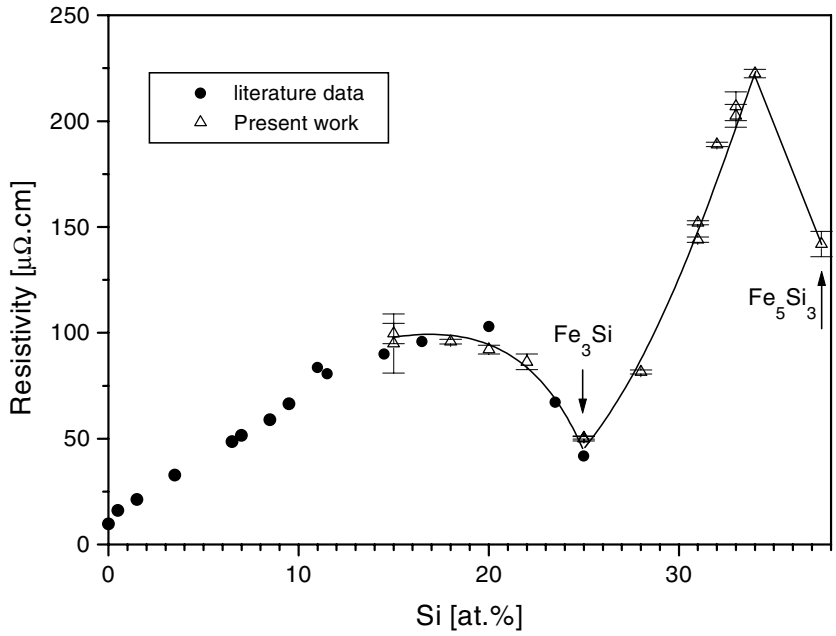

Figure 3. Resistivity versus Si as a function of Si content from literature data and the present work. The solid circles are after Yensen and Corson [27, 28].

the Mooij limit (150 μm) where a change in sign of the TCR is expected. From previous data, the resistivity was expected to have a minimum for the stoichiometric compound Fe_3Si, and this was verified in the present work. It is remarkable that such a high resistivity (>200 $\mu\Omega$ cm), in transition-metal-based compounds, was only observed in bulk amorphous alloys which contain up to six elements strongly differing in atomic radius (transition metals + early transition metals + metalloid). For comparison, the drop in resistivity for the ordered hexagonal Fe_5Si_3 is also plotted. In summary, in spite of a superstructure clearly attested to for contents up to almost 32 at.% Si, the dependence of the resistivity on composition exhibits an evolution characteristic of order–disorder transition. This fact speaks for the hypothesis of a structure consisting of one ordered Fe–Si site and a second disordered $Fe_{(1-y)}Si_y$ site where $y = (4x - 1)/2$.

3.3. Magnetic properties

Both the Curie temperature T_C (figure 4) and the saturation magnetization (figure 5) characteristic of these rapidly quenched alloys have been found to be slightly higher than those reported in the literature in the low-Si-content region. These differences might be attributable to the atomic disordered nature of the rapidly quenched samples—as will be confirmed by ^{57}Fe Mössbauer spectrometry. For Fe_5Si_3 we have obtained a low T_C-value of 378 K, in accordance with the literature [21], while the magnetization was found surprisingly to be higher than that of $Fe_{66.7}Si_{33.3}$ (Fe_2Si). For $x > 25$ at.%, our data show a steep decrease in T_C due to the sample being far from equilibrium (stable compounds with $25 < x < 37.5$ at.% cannot exist). Similarly, the samples having $x < 25$ at.% are closer to the equilibrium phase. This steep decrease can be also observed in a plot of magnetization expressed as the number of Bohr magnetons per Fe atom.

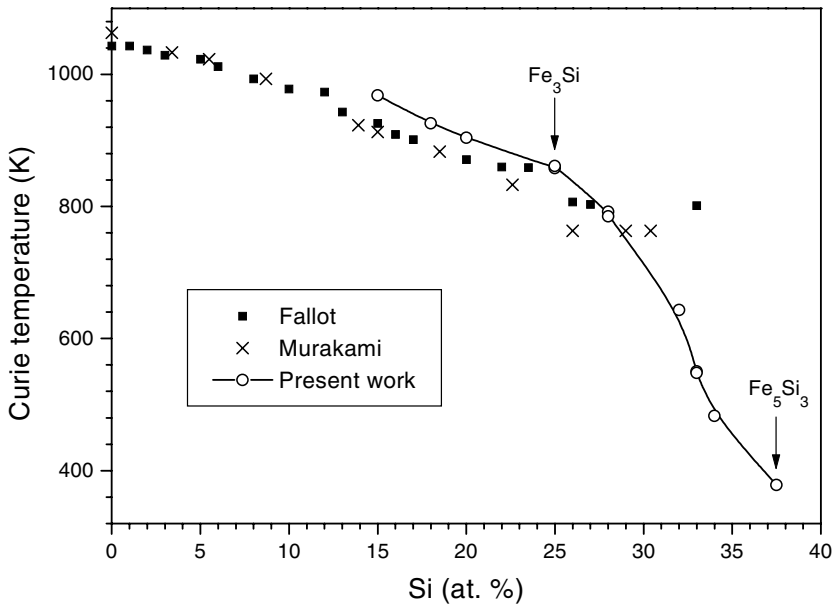

Figure 4. Curie temperature as a function of Si content. The literature data are taken from Murakami and Fallot [3, 4].

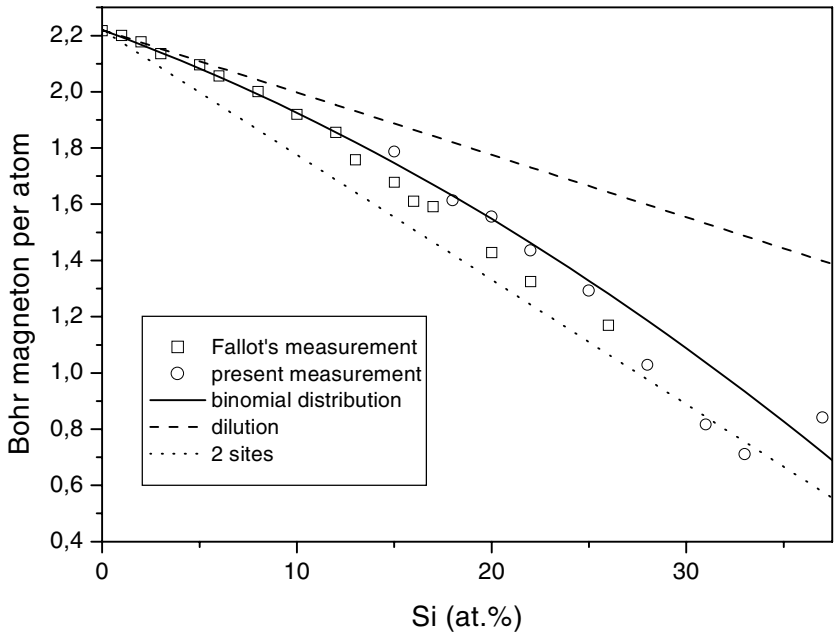

Figure 5. Saturation magnetization versus Si content.

To model the magnetic properties, we consider a random Fe–Si distribution, which is consistent with the short-range order as expected in quenched alloys. The probabilities of Fe having n Si atoms among its z nearest neighbours can be established from the binomial function:

$$P(n) = \frac{z!}{n!(z-n)!}x^n(1-x)^{z-n} \tag{1}$$

where $z = 14$, the coordination number (first and second neighbours) of Fe.

This modelling approach can be thus used to describe the magnetization dependence as a function of the number of Si atoms in the neighbourhood of iron atoms as

$$M(x) = \sum_{n=1}^{z} P_x(n)(M_0 - n\,\delta M(n)). \tag{2}$$

Taking $\delta M = M_0/z$ constant, we obtain a linear decrease of M, typical of a diluted system:

$$M(x) = M_0(1-x). \tag{3}$$

But the experimental data could be better described by considering δM to be linearly dependent on n, as $\delta M = M_0/z + An$.

Assuming that the magnetization of the Fe–Si system vanishes at around 50 at.% Si, i.e. $n = z/2$, then $A = 2M_0/z^2$ is found. Introducing this result in (2) leads to

$$M(x) = M_0\left(1 - \frac{z+2}{z}x - 2\frac{z-1}{z}x^2\right). \tag{4}$$

The Si content dependence of the magnetization is thus calculated and is represented by the full line in figure 5. The experimental data are in good agreement with this model calculation for a Si content up to 25 at.%.

A sensitive deviation is however observed for larger concentrations. This phenomena can be taken into account by a rough model based on two sites as proposed in section 3.2: FeSi and $Fe_{(1-y)}Si_y$. Using the fact that FeSi compound has zero magnetic moment, the first site gives no net magnetic moment. Applying the mixture law to the second site yields

$$M(x) = M_0(\tfrac{1}{2} - x). \tag{5}$$

As seen in figure 5, this two-site-mixture model applies quite well in the highest-concentrations range. A feature of this model is that one considers a zero net moment for the FeSi site, which is only justified if interactions between Fe next-nearest neighbours are weak—which is valid only if the Si concentration is significantly higher than 25 at.%.

3.4. Magnetic anisotropy

The anisotropy constants of Fe–Si are well known from the literature for contents up to 14 at.% Si. It is important to mention that at high Si concentration, only a few values are available. That given for 23.6 at.% Si [32] in the DO_3 phase does not agree with the linear extrapolation of the low-concentration data. The polynomial extrapolation of this curve to higher silicon contents (corresponding to the high-concentration side of the off-stoichiometric DO_3 structure) would suggest K vanishing at around 33–35 at.% Si. Recently, some data published for epitaxially grown films with $x = 25, 33, 42.5$ at.% also departed from this extrapolation [33].

In the present work, the values of the magnetic anisotropy K were obtained from the approach to saturation using different calculation procedures:

(i) by fitting M versus $1/H^2$ [29, 30];
(ii) by fitting the differential permeability versus $1/H^3$ [29]; and
(iii) by extrapolating from the energy of magnetization derived from the field-dependent magnetization.

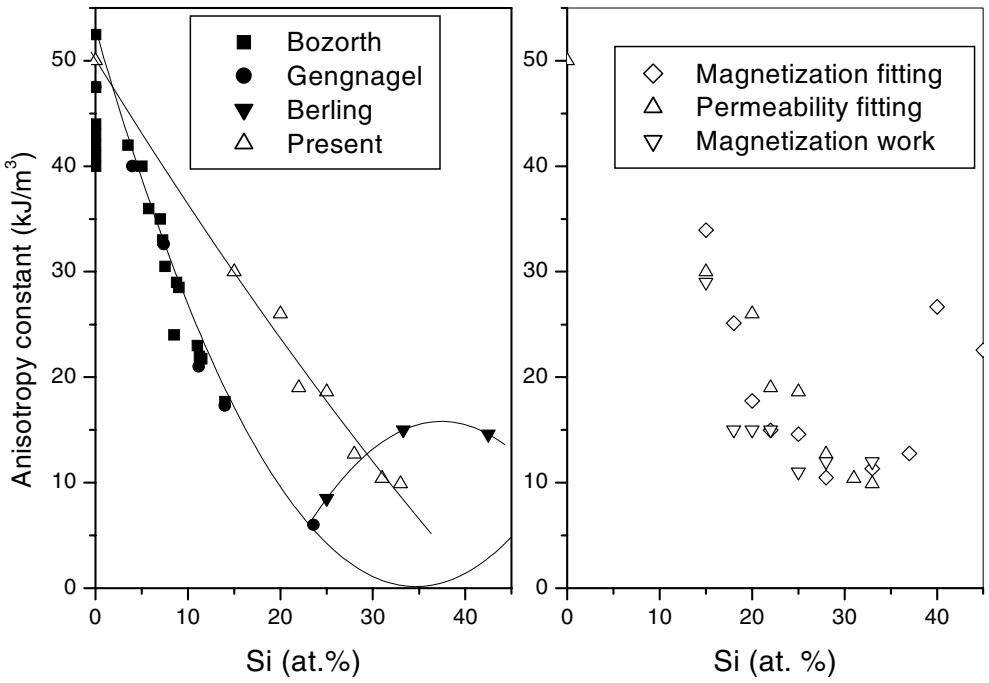

Figure 6. The anisotropy constant as a function of Si content: ■, ingots [31]; ●, thin film [32]; ▼, epitaxial film grown on a Si substrate [33]; △, rapidly quenched (left-hand box). The latter is an average of the values obtained by the three methods (see the right-hand box).

Let us note that, in all of these calculations, the demagnetizing factor has been carefully taken into account and the K-value for pure iron was reproduced fairly accurately. Figure 6 compares the present results to those from the literature: it is concluded that the magnetic anisotropy values of the present nanocrystalline quenched Fe–Si alloys are systematically higher, regardless of the Si content and whatever the calculation procedure is. This tendency can be explained by the magneto-elastic anisotropy introduced during the rapid-quenching process. The crystallite sizes (between 100 and 300 nm) in these alloys are not small enough for the exchange softening to be effective. Moreover, this induced anisotropy cannot be removed by heat treatment without decomposing the metastable structures with more than 28–30 at.% Si into two stoichiometric phases. Although we could not determine the stress-free values, it seems highly probable that the vanishing K-values for high Si content are not realistic.

It can also be observed from figure 6 that K decreases linearly when the Si content increases up to 13 at.% of Si for crystalline Fe–Si alloys and up to 35 at.% of Si for rapidly quenched alloys.

3.5. Magnetostriction

The values collected from the literature for the saturation averaged longitudinal magnetostriction obtained at 300 K for some of the nanocrystalline Fe–Si alloys, λ_s, are plotted in figure 7, versus Si content up to 20 at.% Si, and compared to literature data [33–38]. In the present work, it was not possible to obtain data for these high-Si-content alloys up to 22–34 at.%, either by means of the small-angle magnetization rotation method (due to the brittleness of the present materials) or by usual techniques (due to the ribbon shape). One clearly

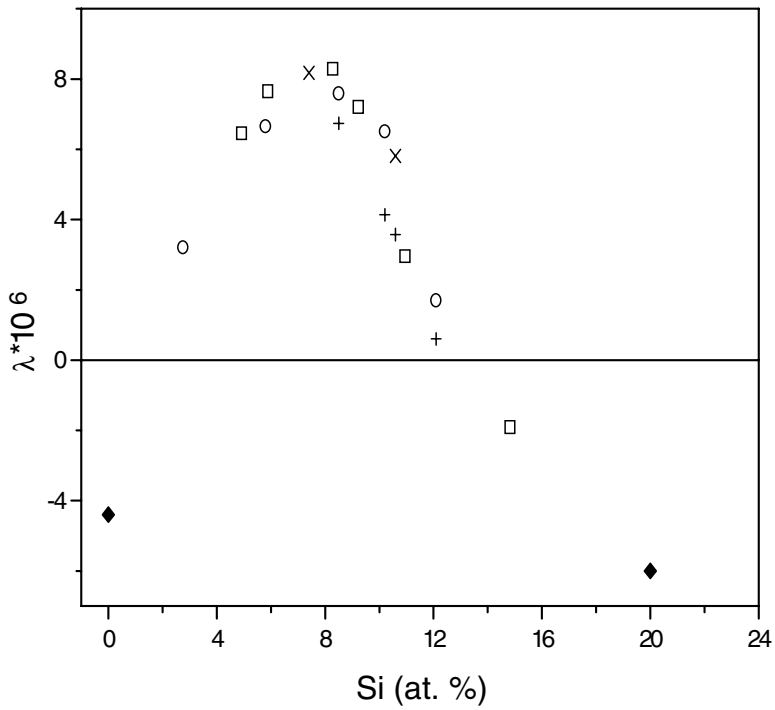

Figure 7. Averaged longitudinal magnetostriction for $Fe_{1-x}Si_x$ alloys: ♦, [32]; □, quenched [33]; ○, quenched [34]; ×, quenched [35]; +, annealed [34, 36].

observes three domains, with negative magnetostriction at $x < 1.5$ at.% and $x > 12.5$ at.% and positive magnetostriction between those two limits in the range $1.5 < x < 12.5$ at.%. It is emphasized that the compositions close to $Fe_{80}Si_{20}$ are of great interest because they correspond to that of the crystalline phase present in the Finemet nanocrystalline alloys. A near-zero magnetostriction value is usually observed for those Fe-containing nanocrystalline alloys with high crystalline fraction [34]. This results from the negative magnetostriction contribution of the Fe–Si crystalline phase, which compensates the positive magnetostriction contribution due to the amorphous Fe-containing remainder. This model is successful with $\bar{\lambda}_s = -6 \times 10^{-6}$, and this is consistent with measured value for $Fe_{80}Si_{20}$, although the λ-value for the remaining amorphous phase is still a controversial point. In order to explain the anisotropy effect discussed above, much effort has to be made to find a method of measuring the magnetostriction coefficient adapted for application to the highest-Si-content alloys.

3.6. ^{57}Fe Mössbauer spectrometry

The local atomic order of the present Fe–Si alloys was studied by ^{57}Fe Mössbauer spectrometry. The evolution of the Mössbauer spectra recorded at 300 K is illustrated in figure 8 as a function of silicon content. For $x < 0.28$, the hyperfine structures of the present nanocrystalline melt-spun ribbons are similar to those observed for usual microcrystalline alloys with the DO_3 structural type. The spectra, which exhibit magnetic sextets with broadened lines, were described by means of a discrete number of magnetic components—values of the isomer shift, quadrupolar shift and hyperfine field—independently refined. The present values estimated at room temperature agree fairly well with those for Fe–Si crystalline alloys with DO_3 structure. It is important to emphasize that the number of iron sites is strongly dependent on the silicon

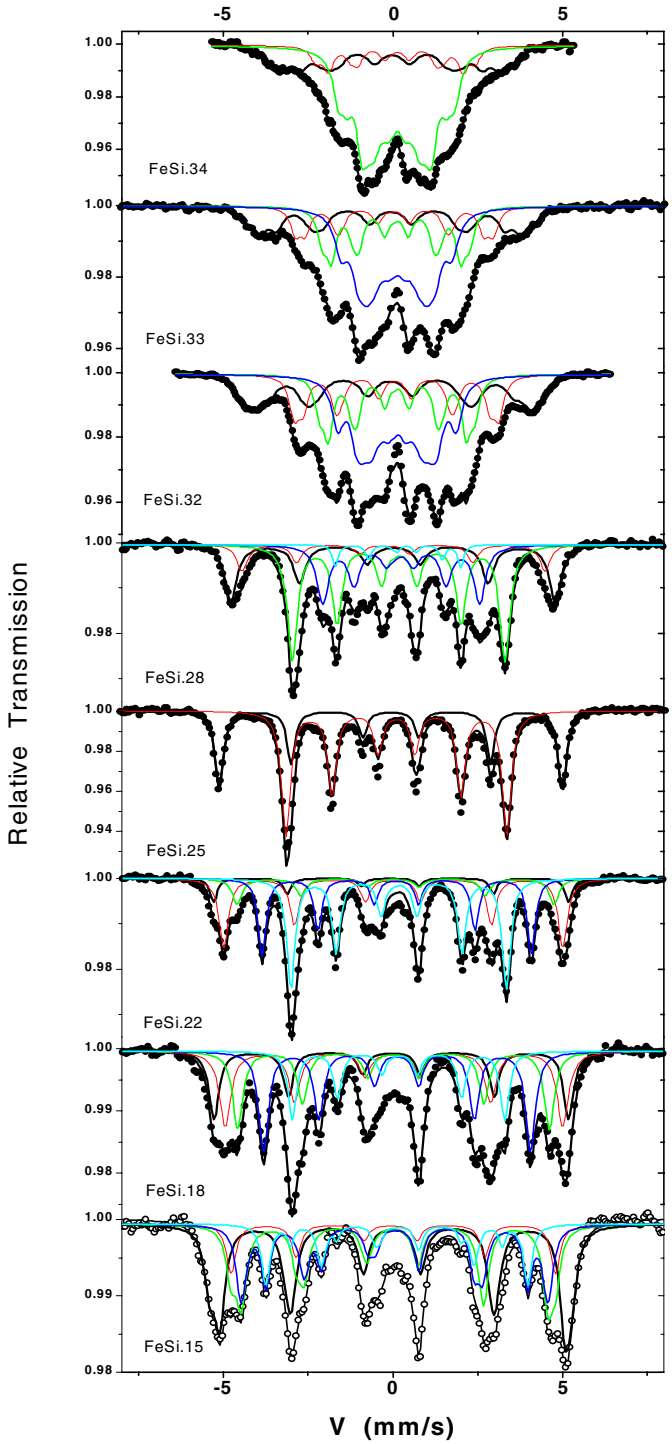

Figure 8. Transmission Mössbauer spectra recorded at 300 K for the present Fe–Si alloys as a function of Si content.

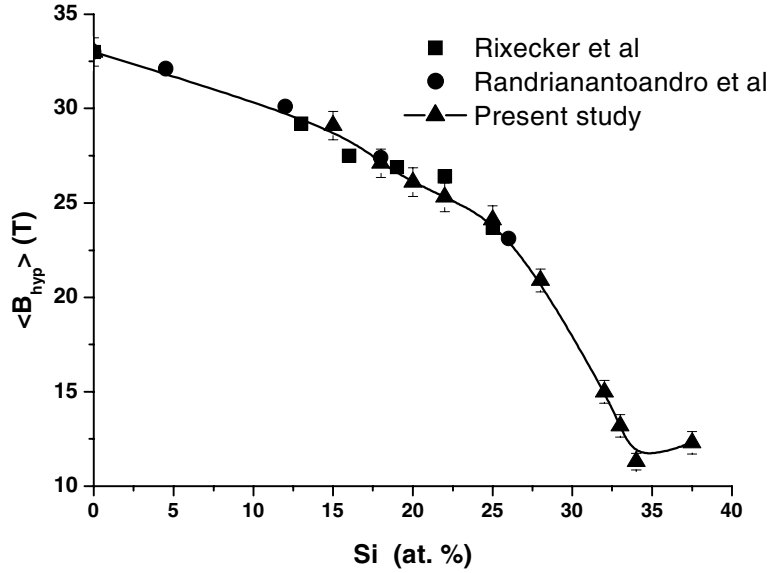

Figure 9. Evolution of the mean hyperfine field estimated at 300 K for $Fe_{1-x}Si_x$ alloys as a function of Si content (the solid curve is a guide for the eye).

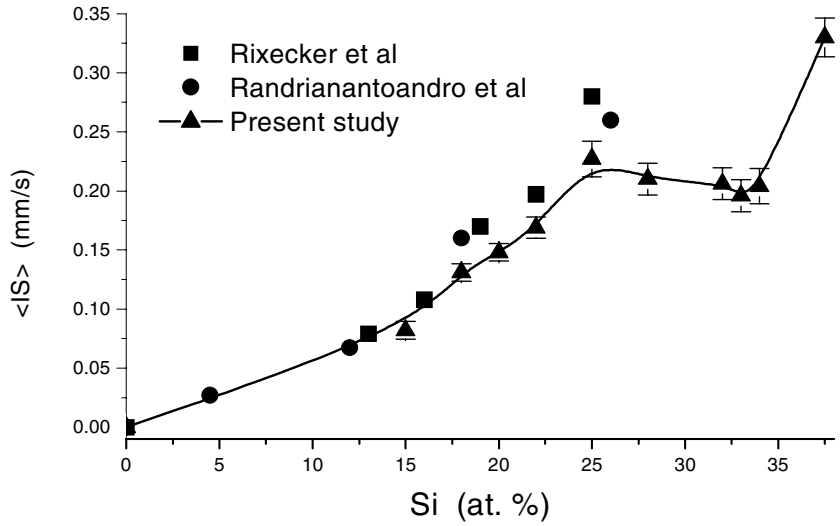

Figure 10. Evolution of the mean isomer shift estimated at 300 K for $Fe_{1-x}Si_x$ alloys as a function of Si content (the solid curve is a guide to the eye).

content for non-stoichiometric Fe–Si alloys which have different structural types, such as A2, B2 or DO_3. The assignment of the various subspectra to the different crystallographic iron sites has already been described in the literature [39–42]. Our results are consistent with previously reported data and it is noticeable that, in spite of the rapid quenching, the 25 at.% Si sample exhibits the two sextets characteristic of the two iron sites. Figures 9 and 10 compare the different dependences of the mean hyperfine-field and isomer shift values versus

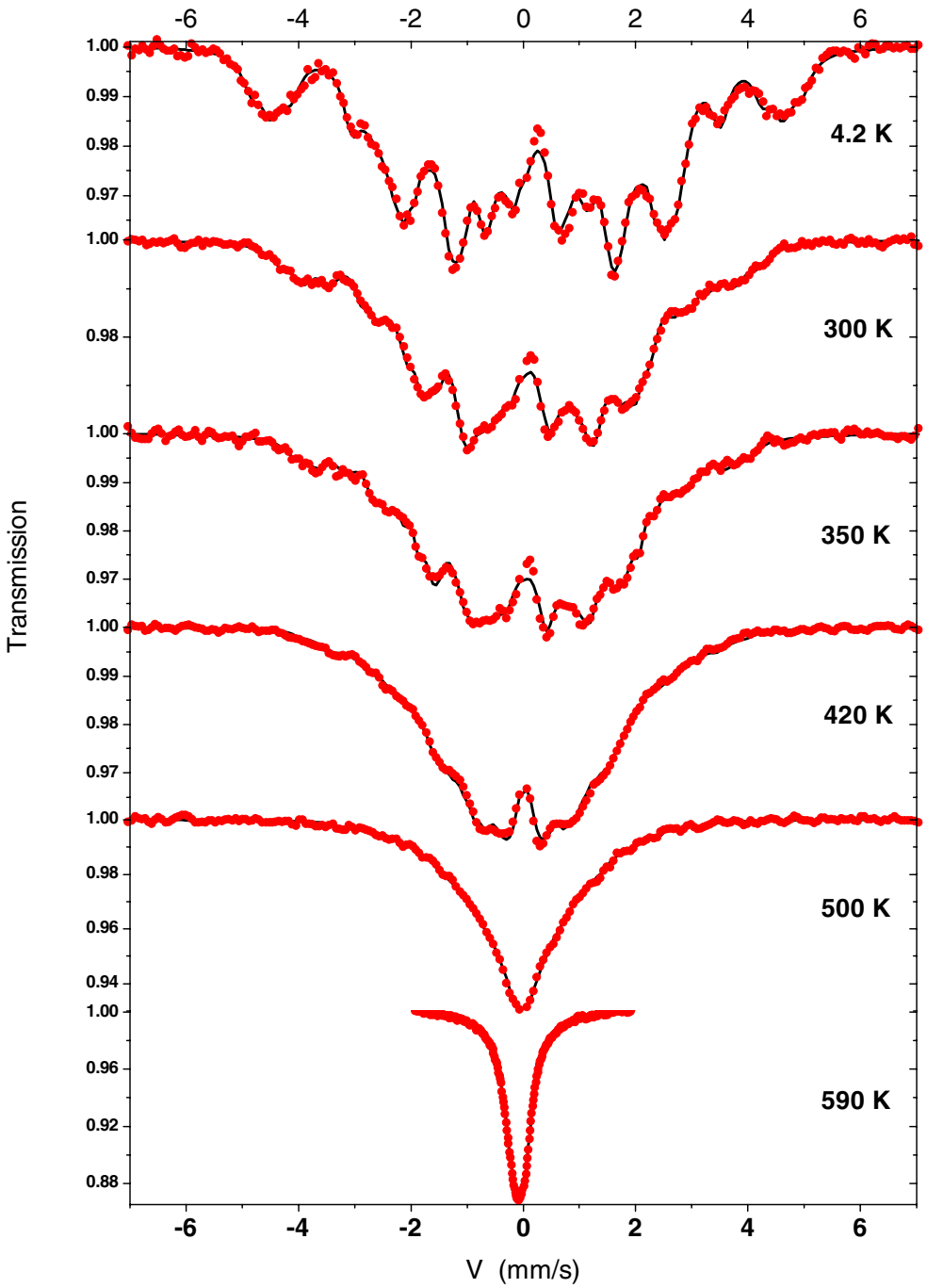

Figure 11. Mössbauer spectra recorded at different temperatures for $Fe_{1-x}Si_x$, $x = 0.33$, alloy.

Si content, respectively. It is thus confirmed well that the present alloys exhibit the same hyperfine characteristics at room temperature as those previously studied with silicon content lower than 25 at.%. The hyperfine field decreases with the Si content only up to 33 at.% Si

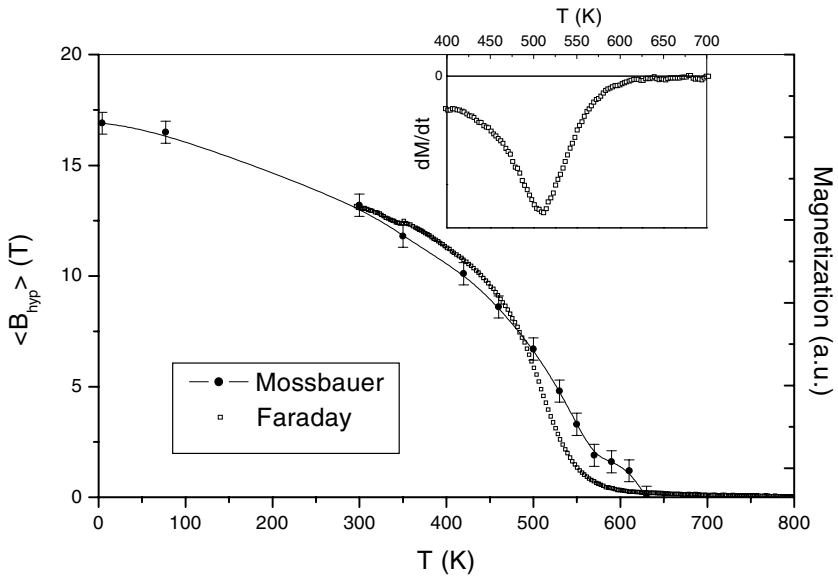

Figure 12. The temperature dependence of the mean hyperfine field of $Fe_{1-x}Si_x$ ($x = 0.33$) alloy (the solid curve is a guide to the eye) compared with the magnetization recorded at 20 kA m^{-1} in a Faraday balance. The inset shows the temperature derivative of the magnetization.

(see figure 9). This behaviour is consistent with that of the magnetization. The isomer shift value increases quasi-linearly when the Si content increases up to 25 at.% and a plateau at Si values between 25 and 30 at.% is observed. It is important to emphasize that the isomer shift is systematically smaller than those previously encountered for Fe–Si microcrystalline alloys when the Si content ranges from 10 to 25 at.%.

The hyperfine structures of several Fe–Si alloys were observed as a function of temperature. Figure 11 shows a series of selected Mössbauer spectra which reveal a progressive collapse of the magnetic hyperfine structure into a single line at high temperature. The complex hyperfine structure matches that of a unique and accurate fitting model consistent with a binomial distribution, due to a random distribution of Fe and Si atoms at the DO_3 sites. Such a description, as previously used by many authors [39–42], leads to a number of sextets which is dependent on the Si content, as shown in figure 8. Hence, only the mean hyperfine field was considered here. Its temperature dependence, shown in figure 12, exhibits an unusual behaviour at temperatures close to the Curie temperature, which is also confirmed by the Faraday balance record of the magnetization as a function of temperature. In particular, the temperature derivative of the magnetization $\partial M/\partial T$ shows a peak with a right-hand side as large as 120 K, typical of a large distribution of the Curie temperature. It is also noticeable that the drop to zero of $\partial M/\partial T$ at 620 K corresponds to that of the hyperfine field. Such a behaviour is consistent with an inhomogeneous distribution of both silicon and iron atoms, i.e. the presence of different Fe–Si clusters whose compositions are not strictly constant.

4. Conclusions

The present work clearly demonstrates that the rapid-quenching technique is appropriate for preparing single-phase Fe–Si alloys up to 32 at.% Si, while two-phase alloys are obtained above this limit. Below 28 at.% Si, these alloys exhibit a DO_3 superstructure (we note that 25 at.% Si

leads to a rather well ordered Fe_3Si alloy) and the Mössbauer parameters are similar to those from the literature including bulk-prepared samples. Highly disordered metastable alloys are obtained when the Si content is in the range from 28 to 34 at.% Si, corresponding to the interval between Fe_3Si and Fe_5Si_3. These metastable alloys exhibit rather contradictory structural and physical properties. On one hand, the XRD spectra attest to the DO_3 superstructure even if the (111) peak is very weak. On the other hand, the high value of the resistivity and the shape of the Mössbauer spectra suggest a high degree of disorder. Indeed, even at 4.2 K, the spectra of the sample with 33 at.% Si cannot be fitted with a discrete number of components and are indicative of a large number of iron sites. The resistivity, which is strongly correlated with the degree of order, is higher than that of binary amorphous alloys but similar to that of some bulk amorphous alloys. Finally, the cost-effective production of these alloys in comparison with $(NiZn)_1Fe_2O_4$ ferrites makes them competitive as regards application for frequencies up to 10 MHz.

References

[1] Barrett W F, Brown W and Hadfield R A 1900 *Sci. Trans. R. Dublin Soc.* **7** p 67
[2] Gumlich E 1918 *Wiss. Abhandl. Phys.-Tech. Reichsanstalt* **4** 68
[3] Murakami T 1921 *Sci. Rep. Tohoku Univ.* **10** 79
[4] Fallot M 1936 *Ann. Phys., Paris* **6** 305
[5] Abdellaoui M, Barradi T and Gaffet E 1992 *J. Physique Coll.* IV **3** 73
[6] Li M, Birringer R, Johnson W L and Shull R D 1994 *Nanostruct. Mater.* **3** 407
[7] Arai K and Tsuya N 1980 *IEEE Trans. Magn.* **16** 126
[8] Faudot F, Railland J F and Bigot J 1989 *Physica Scripta* **39** 263
[9] Sato Turtelli R, Grössinger R, Morais E D, Vo Hong Duong, Wiesinger G, Dahlgren M and Ferrara E 1998 *J. Magn. Magn. Mater.* **177–81** 1389
[10] Takade Y, Abe M, Masuda S and Inagaki J 1988 *J. Appl. Phys.* **64** 5367
[11] Tenwick M J and Davies H A 1984–85 *Int. J. Rapid Solidif.* **1**
[12] Mangin P, Marchal G, Piecuch M and Janot C 1976 *J. Phys. E: Sci. Instrum.* **9** 1101
Mangin P, Marchal G, Piecuch M and Janot C 1976 *Solid State Commun.* **18** 739
[13] Alemada J M *et al* 1983 *J. Magn. Magn. Mater.* **38** 105
[14] Garcia A *et al* 1991 *Mater. Sci. Eng.* A **134** 1394
[15] Schneeweiss O, Jiraskova Y and Havlicek S 1997 *Conf. on Rapidly Quenched and Metastable Materials (RQ9)* ed P Duhaj, P Mrafko and P Svec (Amsterdam: Elsevier) p 434
[16] Yoshisawa Y, Oguma S and Yamauchi K 1988 *J. Appl. Phys.* **64** 6044
[17] Varga L K, Bakos E, Zsoldos E, Kisdi-Koszo E and Kiss L F 1993 *J. Magn. Magn. Mater.* **133** 280
[18] Herzer G 1993 *Phys. Scr.* T **49** 307
[19] Herzer G 1997 *Handbook of Magnetic Materials* vol 10, ed K H J Buschow (Amsterdam: Elsevier) p 415 and references therein
[20] Borrego J M, Conde A, Todd I, Frost M, Davies H A, Gibbs M R J, Garitaonandia J S, Barandiaran J M and Greneche J M 2001 *J. Non-Cryst. Solids* **287** 125
[21] Massalski T B, Murray J L, Bennett L H, Baker H and Kacprzak L (ed) 1986 *Binary Alloy Phase Diagrams* (Metals Park, OH: ASM International) p 1108
[22] Bertotti G and Fiorillo F 1994 Magnetic properties of metals *Landolt–Börnstein New Series* vol 19 (Berlin: Springer) p 33
[23] Varga L K, Mazaleyrat F, Kovac J and Kákay A 2001 *Mater. Sci. Eng.* A **304–6** 946
Varga L K, Mazaleyrat F, Kovac J and Kákay A 2000 *J. Magn. Magn. Mater.* **215–16** 121
[24] Ferrari M and Lutterotti L 1994 *J. Appl. Phys.* **76** 7246 (webpage http://www.ing.unitn.it/∼luttero/maud/)
[25] Teillet J and Varret F *Mosfit Program* University of Le Maine (unpublished)
[26] Farquhar 1945 *J. Iron Steel Inst.* **152** 457
[27] Yensen T D 1915 *Trans. Am. Inst. Electr. Eng.* **34** 23
[28] Corson M G 1928 *Trans. Am. Inst. Min. Met. Eng.* **80** 75
[29] Chihazumi S 1964 *Physics of Magnetism* (New York: Wiley)
[30] Zhou T J, Yu Z and Du Y W 1999 *J. Magn. Magn. Mater.* **202** 354
[31] Bozorth R M 1951 *Ferromagnetism* 3rd edn (New York: IEEE)

[32] Gengnagel H and Wagner H 1961 *Z. Angew. Phys.* **13** 174
[33] Berling D *et al* 1999 *J. Magn. Magn. Mater.* **191** 331
[34] Herzer G 1991 *Mater. Sci. Eng.* A **133** 1
[35] Carr W J and Smoluchovski R 1951 *Phys. Rev.* **83** 1236
[36] Hall R C 1959 *J. Appl. Phys.* **30** 816
[37] Gersdorf R 1961 *Thesis* Amsterdam, quoted in [35]
[38] du Trémolet de Lacheisserie E 1993 *Magnetostriction* (Boca Raton, FL: Chemical Rubber Company) appendix III
[39] Stearns M B 1963 *Phys. Rev.* **129** 1136
[40] Haggstrom L, Granas L, Wappling R and Devanarayanan S 1973 *Phys. Scr.* **7** 125
[41] Rixecker G, Schaaf P and Gonser U 1993 *Phys. Status Solidi* a **139** 309
[42] Randrianantoandro N, Gaffet E, Mira J and Greneche J-M 1999 *Solid State Commun.* **111** 323